Electronic Supporting Information

A generic green solvent concept boosting the power conversion efficiency of all-polymer solar cells to 11%

Zhenye Li [a], Lei Ying* [a], Peng Zhu [a], Wenkai Zhong [a], Ning Li* [b], Feng Liu [c], Fei Huang* [a], and Yong Cao [a]

[a] *Institute of Polymer Optoelectronic Materials and Devices, State Key Laboratory of Luminescent Materials and Devices, South China University of Technology, Guangzhou, 510640, P. R. China. E-mail: msleiying@scut.edu.cn; msfhuang@scut.edu.cn*

[b] *Institute of Materials for Electronics and Energy Technology (i-MEET), FAU Erlangen-Nürnberg, 91058 Erlangen, Germany. E-mail: ning.li@fau.de*

[c] *Department of Physics and Astronomy Shanghai Jiao Tong University, Shanghai 200240, P. R. China*

Experimental Section

Materials

PTzBI-Si and N2200 were synthesised according to procedures reported in the literature.[1] 2-MeTHF, THF, CPME and DBE are purchased from Sigma-Aldrich without further purification.

Fabrication of Polymer Solar Cells

Indium tin oxide (ITO)-coated glass substrates were successively cleaned by sonication in detergent, deionised water, acetone, and isopropyl alcohol and dried in an oven at 75 °C for 6

h prior to use. The substrates were then exposed to oxygen plasma for 1 min and spin coated with PEDOT:PSS (Clevios P VP Al 4083) at 3000 rpm for 30 s. The coated substrates were annealed at 150 °C on a hot plate for 20 min in air to produce 40-nm thin films. After annealing, they were transferred to a glove box under N_2 atmosphere. For 2-MeTHF processed all-PSCs, the total concentration of PTzBI-Si and N2200 was fixed at 6 mg mL^{-1}, and the blend films were obtained by spin coating solutions of the polymers in MeTHF containing DBE (0.5 vol %); to obtain active layer of PTzBI-Si:N2200 with higher thicknesses of 130, 160, 230, and 350 nm, we kept a higher constant total concentration of PTzBI-Si and N2200 of 6 mg mL^{-1} and employed varied rotating speed of 3000, 1800, 1000, and 600 rpm, respectively. For THF processed all-PSCs, the total concentration of PTzBI-Si and N2200 was fixed at 12 mg mL^{-1}, and the blend films were obtained by spin coating solutions of the polymers in THF containing DBE (0.5 vol %); to obtain active layer of PTzBI-Si:N2200 with higher thicknesses of 130, 160, 230, and 350 nm, we kept a higher constant total concentration of PTzBI-Si and N2200 of 12 mg mL^{-1} and employed varied rotating speed of 4000, 2500, 1000, and 600 rpm, respectively. For CPME processed all-PSCs, the total concentration of PTzBI-Si and N2200 was fixed at 9 mg mL^{-1}, and the blend films were obtained by spin coating solutions of the polymers in CPME containing DBE (0.5 vol %); to obtain active layer of PTzBI-Si:N2200 with higher thicknesses of 130, 160, 230, and 350 nm, we kept a higher constant total concentration of PTzBI-Si and N2200 of 9 mg mL^{-1} and employed varied rotating speed of 3000, 2000, 1200, and 600 rpm, respectively. For CB processed all-PSCs, the total concentration of PTzBI-Si and N2200 was fixed at 10.5 mg mL^{-1}, and after spin-coating the solution at 700 rpm for 90 s, the robust film with thickness of about 130 nm was obtained. For DCB processed all-PSCs, the total concentration of PTzBI-Si and N2200 was fixed at 13 mg mL^{-1}, and after spin-coating the solution at 700 rpm for 120 s, the robust film with thickness of about 130 nm was obtained. For CF processed all-PSCs, the total concentration of PTzBI-Si and N2200 was fixed at 7.5 mg mL^{-1}, and after spin-coating

the solution at 900 rpm for 30 s, the robust film with thickness of about 130 nm was obtained. The photoactive layers were then thermally annealed at 110 °C for 10 min, followed by spin coating of a 5-nm layer of PFNDI-Br at 2000 rpm for 30 s to serve as the cathode interface. A 100-nm argentum (Ag) layer was then thermally deposited onto the active layer through a shadow mask in a vacuum chamber with a base pressure of 2×10^{-6} mbar. The effective area of the devices (0.04 cm^2) was determined by the shadow mask.

Fabrication and Characterisation of Charge-Only Devices

The hole mobility was measured in a hole-only device with the configuration of ITO/PEDOT:PSS/active layer/Ag. The electron mobility was measured in an electron-only device with the configuration of ITO/ZnO/active layer/PFNDI-Br/Ag. The ZnO sol-gel is obtained from stirring the solution of 1.0 g Zn(CH3COO)2·2H2O in 10 mL ethylene glycol monomethyl ether and 275 μL ethylenediamine at 60 ºC for 12 h. For 2-MeTHF processed all-PSCs, the total concentration of PTzBI-Si and N2200 was fixed at 6 mg mL^{-1}, and the blend films were obtained by spin coating solutions of the polymers in MeTHF containing DBE (0.5 vol %); to obtain active layer of PTzBI-Si:N2200 with higher thicknesses of 130, 160, 230, and 350 nm, we kept a higher constant total concentration of PTzBI-Si and N2200 of 6 mg mL^{-1} and employed varied rotating speed of 3000, 1800, 1000, and 600 rpm, respectively. For THF processed all-PSCs, the total concentration of PTzBI-Si and N2200 was fixed at 12 mg mL^{-1}, and the blend films were obtained by spin coating solutions of the polymers in THF containing DBE (0.5 vol %); to obtain active layer of PTzBI-Si:N2200 with higher thicknesses of 130, 160, 230, and 350 nm, we kept a higher constant total concentration of PTzBI-Si and N2200 of 12 mg mL^{-1} and employed varied rotating speed of 4000, 2500, 1000, and 600 rpm, respectively. For CPME processed all-PSCs, the total concentration of PTzBI-Si and N2200 was fixed at 9 mg mL^{-1}, and the blend films were obtained by spin coating solutions of the polymers in CPME containing DBE (0.5 vol %); to

obtain active layer of PTzBI-Si:N2200 with higher thicknesses of 130, 160, 230, and 350 nm, we kept a higher constant total concentration of PTzBI-Si and N2200 of 9 mg mL^{-1} and employed varied rotating speed of 3000, 2000, 1200, and 600 rpm, respectively. The mobility μ was determined by fitting the dark current to the model of a single-carrier SCLC, which is described by Equation (1):

$$J = (9/8)\varepsilon_0\varepsilon_r\mu V_{eff}^{\ 2}/d^3, \quad (1)$$

where J is the current density, μ is the charge (hole or electron) mobility at zero field, ε_0 is the permittivity of free space, ε_r is the relative permittivity of the material, d is the thickness of the active layer, and V_{eff} is the effective voltage ($V-V_{bi}$). The charge (hole or electron) mobility was calculated from the y intercept of the J–V curves.

Instruments and Characterisation

The absorption spectra of the film and solution samples were measured using a UV–vis spectrophotometer (HP 8453, photodiode array type) in the wavelength range of 300–1000 nm. PL spectra were recorded on a Jobin-Yvon FluoroMax-4 spectrofluorometer. The current density–voltage (J–V) characteristics were measured using a computer-controlled Keithley 2400 SourceMeter under 1 sun irradiation from an AM 1.5 G solar simulator (Taiwan, Enlitech, SS-F5). The EQE spectra were measured using a commercial EQE system (Taiwan, Enlitech, QE-R3011).

Grazing incidence wide-angle X-ray scattering (GIWAXS)

GIWAXS characterization of the thin films was performed at beamline 7.3.3 of Advanced Light Source, Lawrence Berkeley National Laboratory (LBNL). The X-ray beam energy was 10 keV. The sample to detector distance was ~280 mm calibrated with AgB and the incidence angle was 0.16o normalized by a photodiode. All the GIWAXS signals were recorded in Helium atmosphere with exposure time of 5 s per image using a 2D charge-coupled device

(CCD) detector (Pilatus 2M) with a pixel size of 0.172 mm by 0.172 mm. Thin film samples were spin-coated on PEDOT:PSS/silicon wafer substrates.

Resonant soft X-ray scattering (R-SoXS)

RSoXS was performed at beamline 11.0.1.2 of Advanced Light Source, LBNL. Sample preparation was the same as that of GIWAXS samples. The thin films were floated in deionized water and transferred on silicon nitrile (Si3N4) windows, and subsequently the samples were loaded onto a holder. After the films were dried in air, the holder was transferred into the vacuum chamber for RSoXS. The beam energy was screened ranging from 280 to 290 eV, with a 10 s exposure time per energy. The scattering patterns were collected in vacuum using Princeton Instrument PI-MTE CCD camera with a pixel size of 0.027 mm by 0.027 mm. RSoXS data of each sample were recorded at two sample-to-CCD distance of 50 and 150 mm.

Table S1. Polymer solubility test at different temperatures with certain concentrations in CPME.

Polymer	Total Conc. (mg mL^{-1})	Solubility [a] (120 °C)	Solubility [a] (60 °C)	Solubility [a] (R.T. ≈ 25 °C)
PTzBI-Si	20	+++	+++	++
N2200	10	+++	++ [c]	+ [c]
PTzBI-Si:N2200 (1:0.5)	15	+++	+++	++ [c]

[a] +++ represents good solubility, ++ represents soluble but with high viscosity, + represents forming nearly gel state;[2] [c] stirred at 120 °C for 30 min and then cooled down to 60 °C or R.T.

Table S2. Photovoltaic parameters of all-PSCs with the active layers processed by various solvent and solvent additives.

Solvent	Solvent additive	V_{OC} (V)	J_{SC} (mA cm^{-2})	FF (%)	PCE (%)
2-MeTHF	N/A	0.87	15.8	71.1	9.8
	0.5% DBE	0.86	15.7	72.5	9.8
	0.5% DPE	0.84	15.1	71.9	9.2
THF	N/A	0.89	11.7	61.9	6.5
	0.5% DBE	0.85	13.6	63.4	7.4
	0.5% DPE	0.86	13.4	63.1	7.2
CPME	N/A	0.87	16.1	70.3	9.9
	0.5% DBE	0.86	16.4	77.1	10.9
	1% DBE	0.84	16.0	78.4	10.5
CB	N/A	0.87	2.2	58.5	1.2
DCB	N/A	0.87	2.1	61.5	1.1
CF	N/A	0.86	9.1	64.7	5.1

Table S3. Photovoltaic parameters of all-PSCs thermal anneal (TA) for 10 min at different temperature.

Solvent	Thermal annealing	V_{OC} (V)	J_{SC} (mA cm^{-2})	FF (%)	PCE (%)
2-MeTHF [a]	100 ℃/10min	0.87	15.4	71.2	9.5
	110 ℃/10min	0.87	15.8	71.1	9.8
	120 ℃/10min	0.86	15.7	72.0	9.7
THF [a]	100 ℃/10min	0.85	13.3	62.9	7.1
	110 ℃/10min	0.85	13.6	63.4	7.4
	120 ℃/10min	0.85	13.5	61.0	7.0
CPME [a]	100 ℃/10min	0.86	16.7	75.0	10.7
	110 ℃/10min	0.86	16.4	77.1	10.9
	120 ℃/10min	0.85	16.0	76.7	10.4

[a] With 0.5vol%DBE.

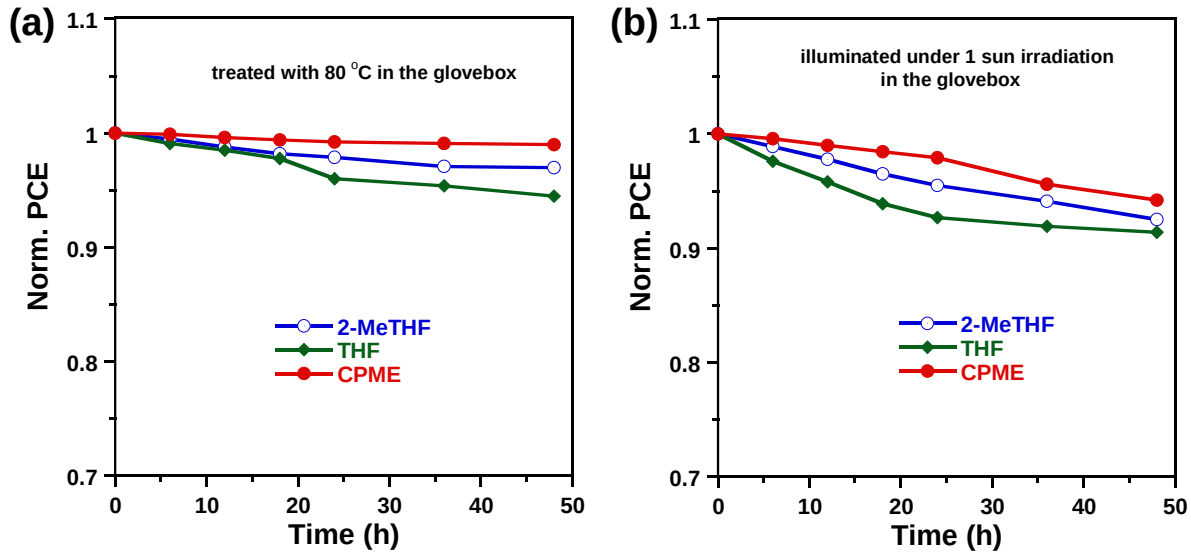

Fig. S1. Normalized PCE of 2-MeTHF, THF and CPME processed all-PSCs blend films treated with 80 °C (a) and illuminated under 1 sun irradiation in the glovebox for different time.

Table S4. Photovoltaic parameters of 2-MeTHF processed all-PSCs with different thickness.

Solvent	Thickness (nm)	V_{OC} (V)	J_{SC} (mA cm^{-2})	FF (%)	PCE (%)
2-MeTHF [a]	100	0.88	15.6	69.8	9.6
	130	0.87	15.6	73.1	9.9
	160	0.87	15.7	68.1	9.3
	200	0.87	15.1	65.5	8.6
	230	0.86	14.6	58.4	7.3
	300	0.86	16.7	50.7	7.3
	350	0.85	17.0	44.7	6.5

[a] With 0.5vol%DBE.

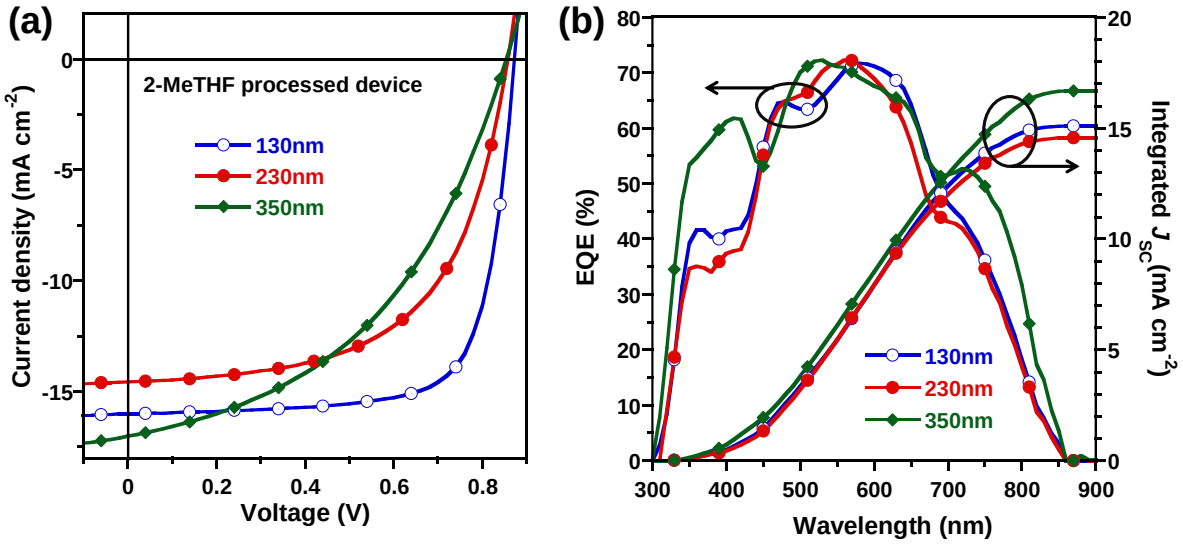

Fig. S2. (a) *J-V* characteristics and (b) EQE spectra of 2-MeTHF processed all-PSCs with different thickness.

Table S5. Photovoltaic parameters of THF processed all-PSCs with different thickness.

Solvent	Thickness (nm)	V_{OC} (V)	J_{SC} (mA cm^{-2})	FF (%)	PCE (%)
THF [a]	100	0.85	12.0	70.7	7.2
	130	0.85	13.6	63.4	7.4
	160	0.85	13.4	63.1	7.2
	200	0.85	12.5	62.1	6.7
	230	0.85	12.2	56.9	6.0
	300	0.85	12.3	55.0	5.8
	350	0.85	12.2	54.1	5.6

[a] With 0.5vol%DBE.

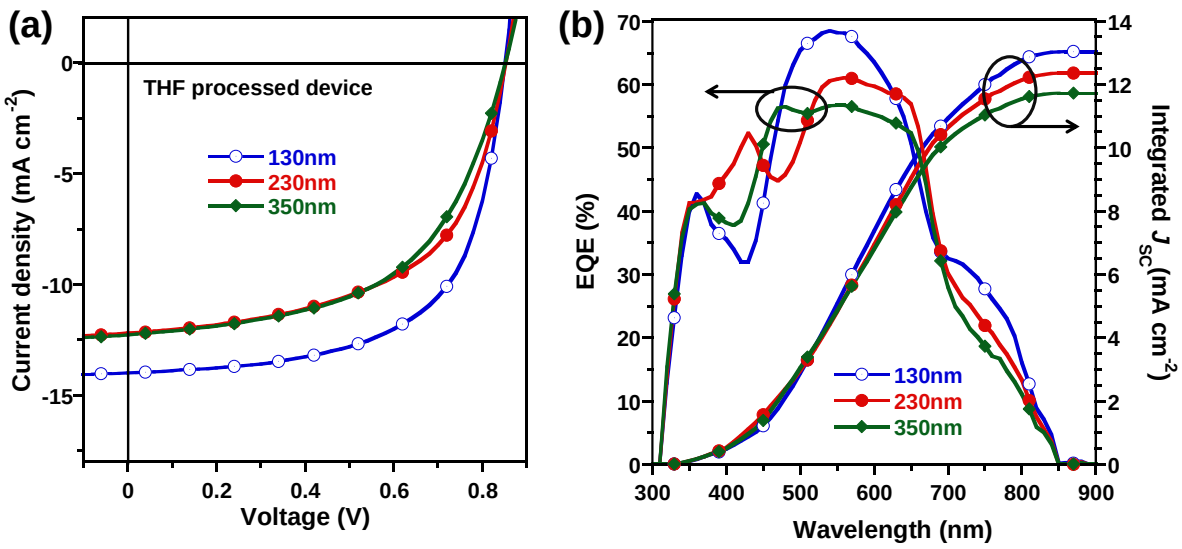

Fig. S3. (a) *J-V* characteristics and (b) EQE spectra of THF processed all-PSCs with different thickness.

Table S6. Photovoltaic parameters of CPME processed all-PSCs with different thickness.

Solvent	Thickness (nm)	V_{OC} (V)	J_{SC} (mA cm^{-2})	FF (%)	PCE (%)
CPME [a]	100	0.85	16.0	77.3	10.5
	130	0.86	16.5	77.9	10.9
	160	0.86	16.0	76.7	10.4
	200	0.86	15.7	73.4	9.9
	230	0.86	15.9	71.3	9.7
	300	0.84	16.8	68.0	9.5
	350	0.84	18.6	58.0	9.1

[a] With 0.5vol%DBE.

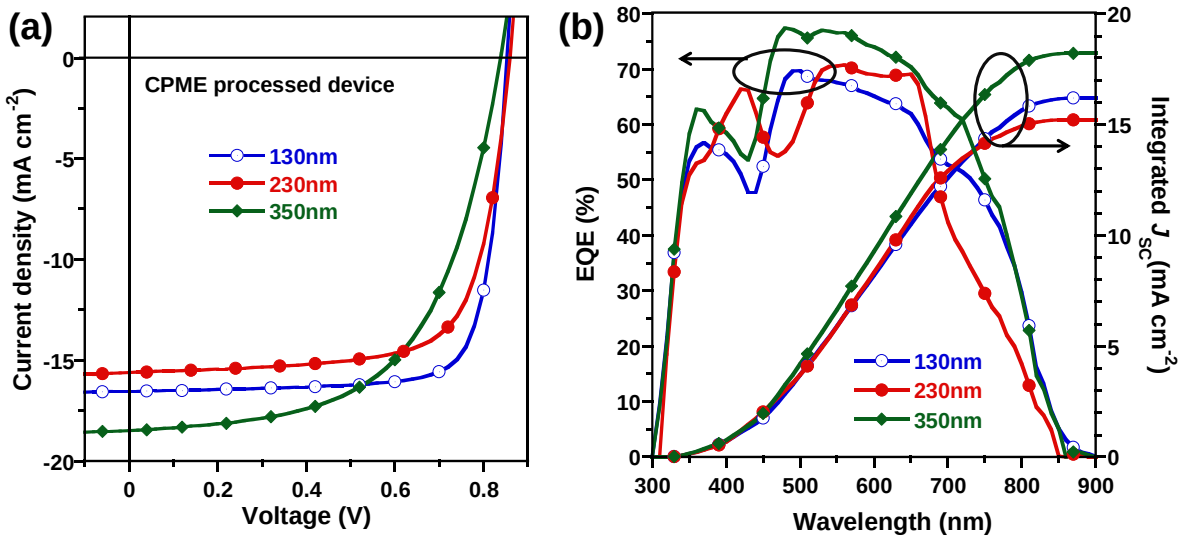

Fig. S4. (a) J-V characteristics and (b) EQE spectra of CPME processed all-PSCs with different thickness.

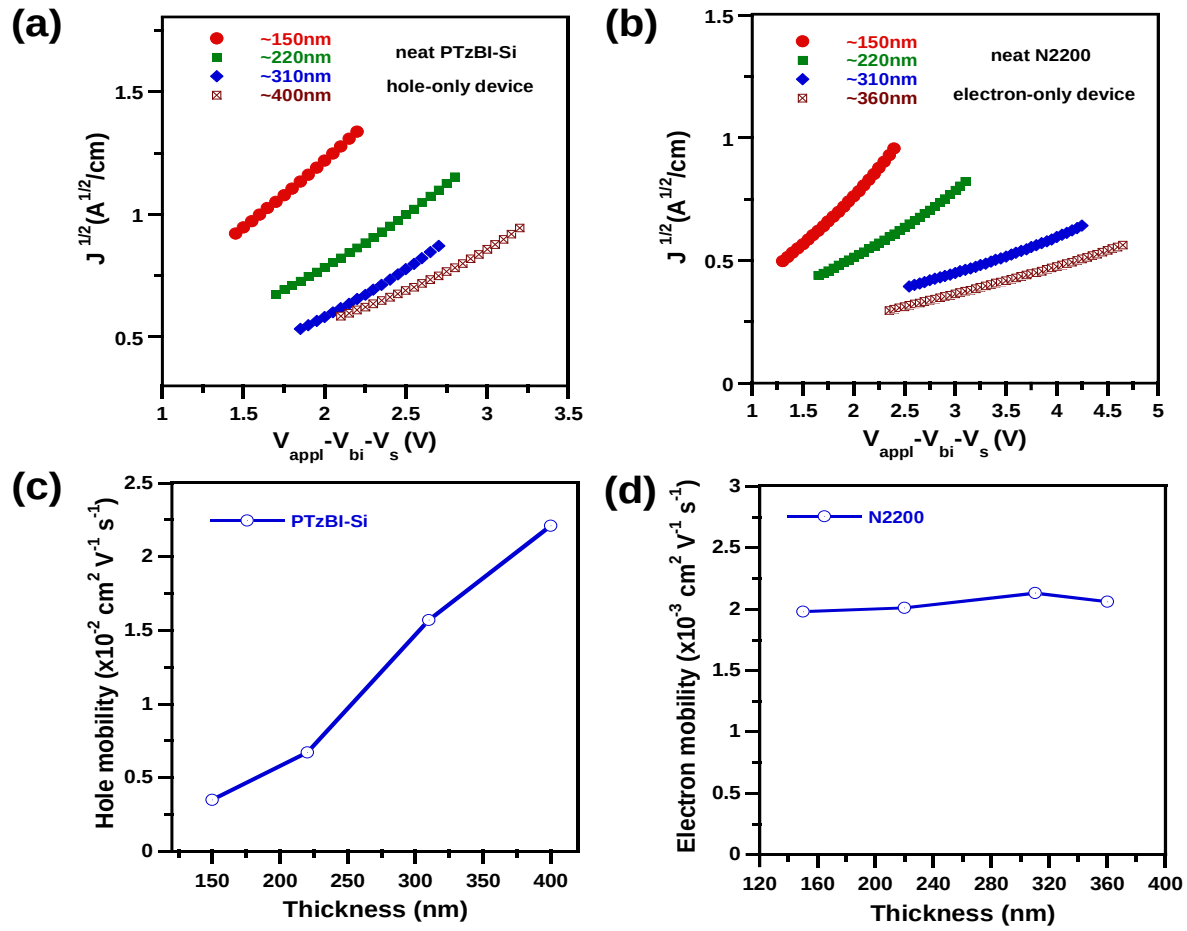

Fig. S5. SCLC hole and electron mobility for PTzBI-Si (a) and N2200 (b); hole mobility and electron mobility versus thickness characteristics for PTzBI-Si (c) and N2200 (d).

Table S7. SCLC electron (hole) mobility measurements for PTzBI-Si and N2200 with different thickness.

Polymer [a]	μ_h (cm^2 V^{-1} s^{-1})	μ_e (cm^2 V^{-1} s^{-1})	Thickness (nm)
PTzBI-Si	3.52×10^{-3}	/	~150
	6.73×10^{-3}	/	~220
	1.57×10^{-2}	/	~310
	2.21×10^{-2}	/	~400
N2200	/	1.98×10^{-3}	~150
	/	2.01×10^{-3}	~220
	/	2.13×10^{-3}	~310
	/	2.06×10^{-3}	~360

[a] All of the blend films are treated with 110 °C for 10 min.

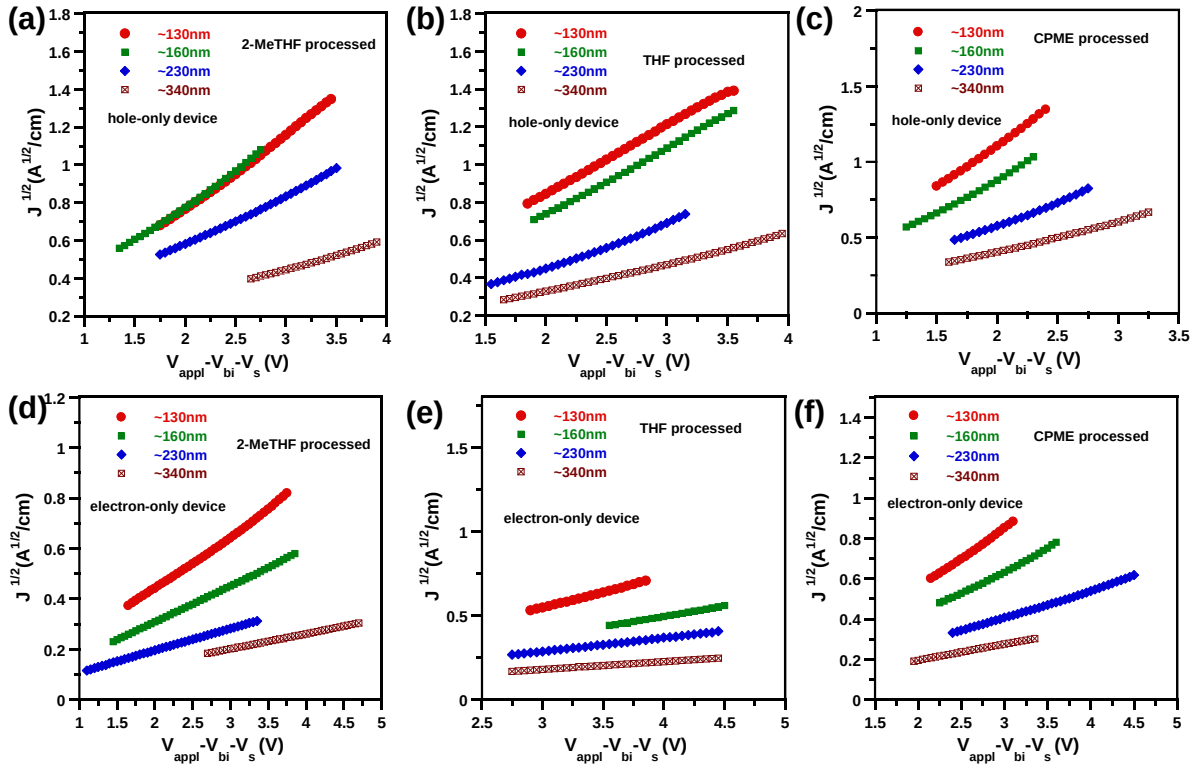

Fig. S6. SCLC hole and electron mobility for 2-MeTHF (a, d), THF (b, e) and CPME (c, f) processed devices with different thickness.

Table S8. SCLC electron (hole) mobility measurements for 2-MeTHF, THF and CPME processed devices with different thickness.

Solvent [a]	μ_h (cm^2 V^{-1} s^{-1})	μ_e (cm^2 V^{-1} s^{-1})	μ_h/μ_e	Thickness (nm)
2-MeTHF	1.29×10^{-3}	0.32×10^{-3}	4.03	~130
	1.88×10^{-3}	0.30×10^{-3}	6.27	~160
	2.68×10^{-3}	0.31×10^{-3}	8.65	~230
	3.04×10^{-3}	0.34×10^{-3}	8.94	~340
THF	0.96×10^{-3}	0.25×10^{-3}	3.84	~130
	1.38×10^{-3}	0.21×10^{-3}	6.57	~160
	1.91×10^{-3}	0.20×10^{-3}	9.55	~230
	2.12×10^{-3}	0.18×10^{-3}	11.78	~340
CPME	2.34×10^{-3}	0.65×10^{-3}	3.60	~130
	2.65×10^{-3}	0.66×10^{-3}	4.02	~160
	3.76×10^{-3}	0.73×10^{-3}	5.15	~230
	3.91×10^{-3}	0.75×10^{-3}	5.21	~340

[a] All of the blend films are treated with 110 °C for 10 min.

Charge generation, recombination and extraction

To investigate the photoinduced carrier generation and charge collection behavior of 2-MeTHF, THF and CPME processed all-PSCs, we plotted the dependence of the photocurrent density (J_{ph}) on the effective voltage (V_{eff}) under illumination at 100 mW cm^{-2} on a double-logarithmic scale (**Fig. S7a**). The photocurrent density (J_{ph}) is defined by $J_{ph} = J_L - J_D$, where J_L and J_D stand for the current densities measured under illumination and in the dark, respectively. The effective voltage (V_{eff}) is defined as $V_{eff} = V_{bi} - V_{appl}$, where V_{bi} is the voltage when $J_{ph} = 0$ (the built-in voltage) and V_{appl} is the applied voltage.[3,4] As depicted in **Fig. S7a**,

J_{ph} increased linearly when V_{eff} was below 0.2 V and tended to saturate at a sufficiently high V_{eff} above 2 V, suggesting that sweep out all of the generated carriers to the electrodes at an effective voltage above 2 V. Therefore, the maximum photoinduced carrier generation rate G_{max} can be calculated from the equation $G_{max} = J_{sat}/(q \cdot L)$, where q is the elementary charge and L is the active-layer thickness, and the charge collection capacity P_C can be calculated using the equation $P_C = J_{ph}/J_{sat}$. As shown in **Table S9** (in the ESI), the CPME processed all-PSCs simultaneously exhibited the highest values of G_{max} (8.73×10^{27} m^{-3} s^{-1}) and P_C (0.986), indicating that the device possessed good carrier generation and collection ability and thus high J_{SC} values.

The charge transfer properties of 2-MeTHF, THF and CPME processed all-PSCs were examined by measuring the photoluminescence (PL) spectra of PTzBI-Si:N2200 blend films excited at both 550 and 740 nm.[5] The PL emissions from PTzBI-Si (excited at 550 nm) and N2200 (excited at 740 nm) were quenched more completely in the CPME processed all-PSCs than that in the 2-MeTHF and THF processed all-PSCs (**Fig. S7b**), indicating the more effective charge carrier dissociation of the generated excitons in this device. Due to the limited exciton diffusion length, efficient PL quenching in the CPME processed all-PSCs also implies that donor (PTzBI-Si) and acceptor polymers (N2200) are mixed on the sub-10 nm length scale.[6] The J_{SC} versus light intensity (P_{light}) characteristics were measured for 2-MeTHF, THF and CPME processed all-PSCs to investigate the charge recombination dynamics in the photoactive layer, and the relevant plots and parameters are shown in **Fig. S7c**. For organic solar cells, it is well established that the power-law dependence of J_{SC} on the illumination intensity can generally be expressed as $J_{SC} \propto (P_{light})^S$, where P_{light} is the light intensity and S is the exponential factor, which is close to unity when bimolecular recombination is weak in the device.[7,8] The extracted S value was 0.99 for CPME processed all-PSCs (while 0.94 and 0.90 for 2-MeTHF and THF processed all-PSCs, respectively), suggesting that the bimolecular recombination was weaker in CPME processed all-PSCs than

that in 2-MeTHF and THF processed all-PSCs. This observation was consistent with the high FF values (>77%) of the corresponding all-PSCs. It is well known that the V_{OC} depends on the natural logarithm of P_{light} provided the slope value with units of kT/q, where k is the Boltzmann constant, T is temperature, and q is the elementary charge. A slope of kT/q is expected for bimolecular recombination, whereas a strong dependence of V_{OC} on the light intensity ($2kT/q$) is characteristic of monomolecular or trap-assisted recombination.[9] As shown in **Fig. S7d**, the observed slopes of the 2-MeTHF, THF and CPME processed all-PSCs were 1.46, 1.64 and 1.39 kT/q, respectively, indicating that the other recombination mechanisms (except for bimolecular recombination) such as monomolecular or trap-assisted recombination are effectively suppressed in CPME processed all-PSCs. The FF–P_{light} characteristics are plotted in **Fig. S7e**. In the low-P_{light} regime, the CPME processed all-PSCs exhibited higher FF than 2-MeTHF and THF processed all-PSCs, indicating weaker bimolecular recombination in this device.

Fig. S7f shows the dark *J*–*V* curves for 2-MeTHF, THF and CPME processed all-PSCs. Fitting the dark *J*–*V* curves by a one-diode equivalent circuit,[10] the diode ideality factor n was calculated to be 1.74, 1.79 and 1.67 for 2-MeTHF, THF and CPME processed all-PSCs, respectively. The lower ideality factor of CPME processed all-PSCs is considered to originate from weaker recombination induced by defect states. Moreover, according to the *J*–*V* characteristics measured in the dark (**Table S10**, ESI), the CPME processed all-PSCs exhibited a much lower series resistance (R_s = 1.10 Ω cm^2) and comparably high parallel device resistance (R_p = 5.83×10^4 Ω cm^2) than those of 2-MeTHF (R_s = 2.37 Ω cm^2 and R_p = 6.91×10^4 Ω cm^2) and THF (R_s = 2.44 Ω cm^2 and R_p = 3.79×10^4 Ω cm^2) processed all-PSCs. We also calculated the FF including the series and parallel resistance losses (FF_{SP}) using the equivalent circuit model,[11,12] and obtained values were 71.61%, 64.14% and 76.20% for 2-MeTHF, THF and CPME processed all-PSCs, respectively (**Table S11**, ESI). These calculated FF values are in good agreement with that obtained from the *J*–*V* plots.

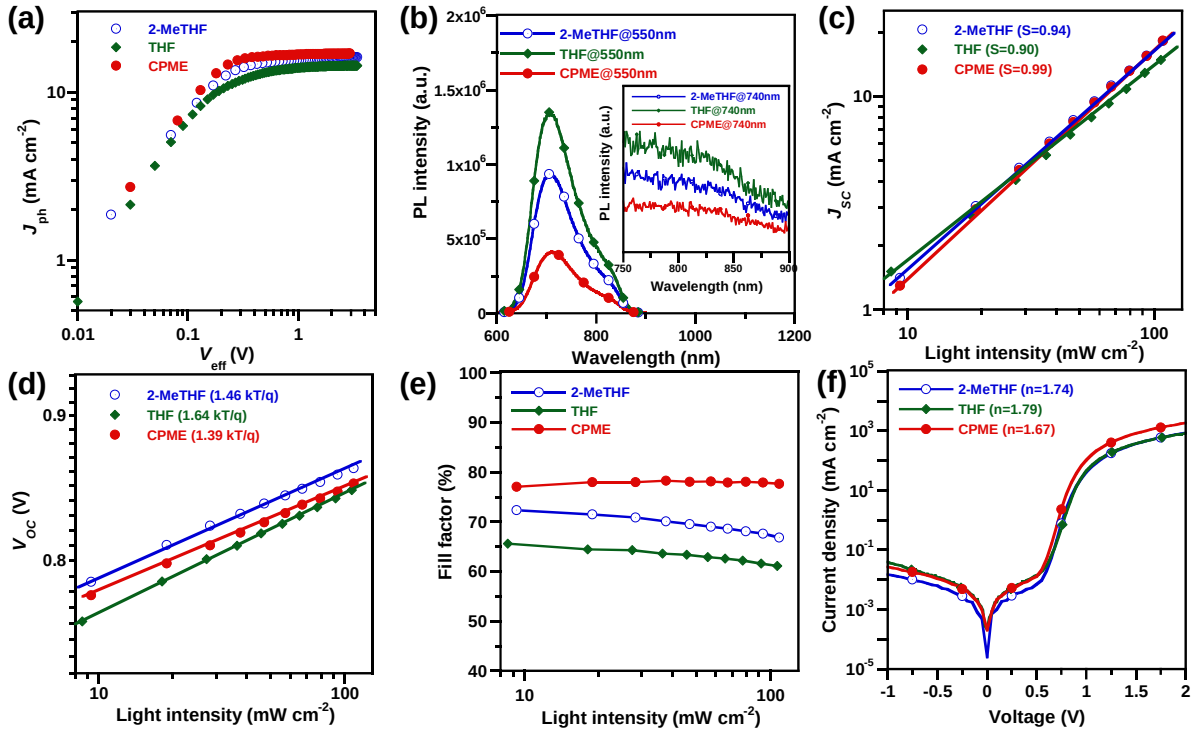

Fig. S7. (a) J_{ph}–V_{eff} curves, (b) PL spectra, (c-e) J_{SC}, V_{OC} and FF versus light intensity (P_{light}) characteristics, (f) dark J–V curves and corresponding ideality factors (fitted by a one-diode equivalent circuit) for 2-MeTHF, THF and CPME processed all-PSCs.

Table S9. Relevant parameters obtained from J_{ph}–V_{eff} curves.

Solvent [a]	J_{ph} [b] (mA cm^{-2})	J_{sat} (mA cm^{-2})	G_{max} (m^{-3} s^{-1})	P_C [b]	L (nm)
2-MeTHF	15.46	16.10	8.27×10^{27}	0.960	~130
THF	13.88	14.47	7.43×10^{27}	0.959	~130
CPME	16.76	17.01	8.73×10^{27}	0.986	~130

[a] All of the blend films treated with 110 °C for 10 min ; [b] At the condition of $V_{eff} = V_0 - V_{appl}$ (V_{appl} = 0, under short-circuit condition).

Table S10. Series resistance (R_S), shunt resistance (R_P), and the simulated ideality factor n for 2-MeTHF, THF and CPME processed devices obtained from dark *J–V* characteristics.

Device	R_S [a] (Ω cm^{-2})	R_P [a] (Ω cm^{-2})	n
2-MeTHF	2.37	6.91×10^4	1.74
THF	2.44	3.79×10^4	1.79
CPME	1.10	5.83×10^4	1.67

[a] R_S and R_P were were calculated around 2 V and 0 V, respectively, from the dark *J–V* characteristics. [b] n was estimated by fitting of a one diode replacement circuit for the dark *J–V* characteristics.

Table S11. Calculated photovoltaic parameters for 2-MeTHF, THF and CPME processed devices.

Device	v_{oc} [b]	R_S^* [a] (Ω cm^{-2})	R_P^* [a] (Ω cm^{-2})	r_s [b]	r_p [b]	FF_0 [b] (%)	FF_S [b] (%)	FF_{SP} [b] (%)
2-MeTHF	19.11	4.08	1.53×10^3	0.075	28.87	80.17	73.53	71.61
THF	18.36	9.47	1.11×10^3	0.152	17.83	79.60	66.73	64.14
CPME	19.68	2.03	3.64×10^3	0.040	71.48	80.58	77.06	76.20

[a] R_S^* and R_P^* were obtained from illuminated *J–V* characteristics. [b] According to an equivalent circuit model reported by Kippelen et al., the upper-limit fill factor (FF_0), Rs-only-influenced fill factor (FF_S), and both *Rs*- and *Rp*-influenced fill factor (FF_{SP}) can be calculated as follows,

$FF_0 = [v_{oc} - \ln(v_{oc} + 0.72)]/(v_{oc}+1)$, $(R_S = 1/R_P = 0)$

$FF_S = FF_0\,(1 - 1.1\,r_s) + 0.19\,r_s^2$, $(0 \le r_s \le 0.4,\ 1/r_p = 0)$

$FF_{SP} = FF_S\,[1 - (v_{oc} + 0.7)*FF_S/(v_{oc}* r_p)]$, $(0 \le r_s + 1/rp \le 0.4)$

Where $v_{oc} = qV_{OC}/nkT$, q is the elementary charge, n is the ideality factor of the diode, and k is the Boltzmann's constant. r_s and r_p are normalized series and shunt resistance ($r_s = R_S * J_{SC}/V_{OC}$, $r_p = R_P * J_{SC}/V_{OC}$).

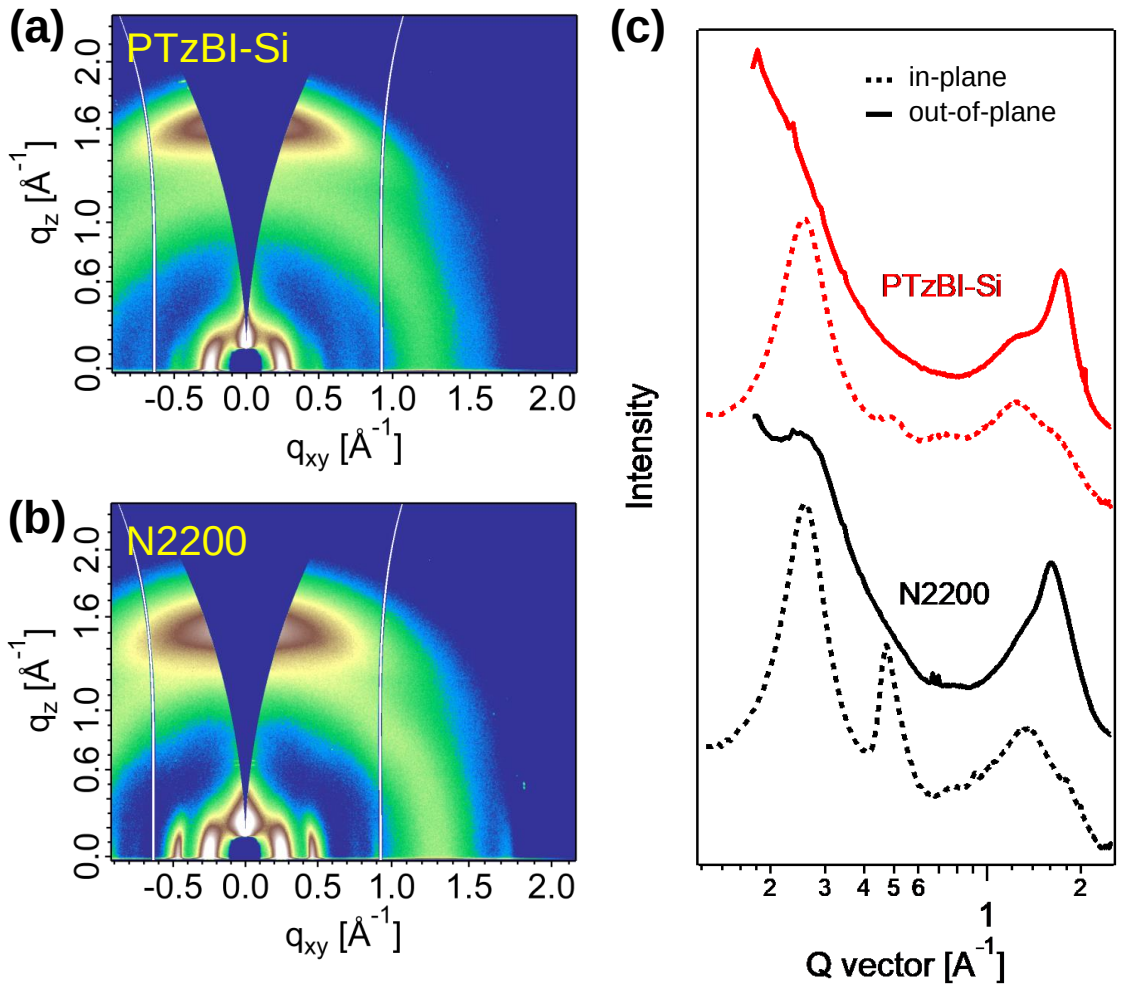

Fig. S8. GIWAXS patterns of neat PTzBI-Si (a) and N2200 (b) films; one-dimensional integrated scattering profiles for the corresponding films (c).

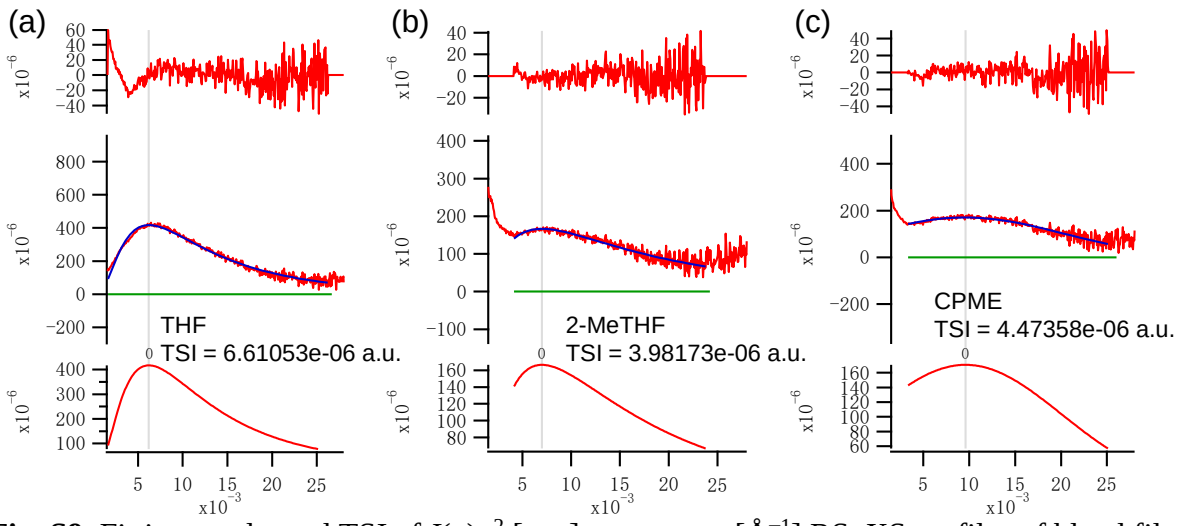

Fig. S9. Fitting results and TSI of $I(q)q^2$ [a.u.] versus to q [Å^{-1}] RSoXS profiles of blend films processed with THF, 2-MeTHF, and CPME.

Table S12. Photovoltaic parameters of all-PSCs measured under AM1.5 Illumination at 100 mW/cm^2.

D:A	Solvent	V_{OC} (V)	J_{SC} [d] (mA cm^{-2})	$J_{SC, EQE}$ [e] (mA cm^{-2})	FF (%)	PCE$_{avg}$ [f] (%)	PCE$_{max}$ (%)
PTB7-Th:N2200 [a]	2-MeTHF	0.80	14.6±0.4	14.1	51.9±0.8	5.9±0.2	6.1
	THF	0.80	13.5±0.5	13.4	48.6±0.6	5.2±0.3	5.5
	CPME	0.80	14.8±0.5	14.5	57.5±0.7	6.8±0.2	6.9
J51:N2200 [b]	2-MeTHF	0.83	14.9±0.4	14.5	60.8±0.9	7.5±0.2	7.7
	THF	0.82	14.1±0.3	13.5	61.3±0.8	6.9±0.2	7.1
	CPME	0.83	15.6±0.4	15.3	67.7±0.5	8.4±0.2	8.6
PTzBI:N2200 [c]	2-MeTHF	0.84	15.4±0.5	15.0	68.5±0.5	8.9±0.2	9.1
	THF	0.84	11.9±0.4	11.7	65.9±0.8	6.5±0.3	6.8
	CPME	0.84	16.1±0.3	15.8	73.1±0.7	9.7±0.2	9.9

[a] PTB7-Th:N2200 = 2:1 (wt:wt) without thermal annealing (TA). [b] J51:N2200 = 2:1 (wt:wt) treated with 110 °C for 10 min. [c] PTzBI:N2200 = 2:1 (wt:wt) treated with 130 °C for 10 min. [d] Obtained from *J*–*V* measurements. [e] Obtained from the integration of EQE spectra. [f] The PCE values are obtained from 12 separate devices.

References

1 (a) B. Fan, L. Ying, P. Zhu, F. Pan, F. Liu, J. Chen, F. Huang, Y. Cao, *Adv. Mater.*, 2017, **29**, 1703906; (b) H. Yan, Z. Chen, Y. Zheng, C. Newman, J. R. Quinn, F. Dotz, M. Kastler, A. Facchetti, *Nature*, 2009, **457**, 679.

2 Y. Ji, C. Xiao, Q. Wang, J. Zhang, C. Li, Y. Wu, Z. Wei, X. Zhan, W. Hu, Z. Wang, R. A. Janssen and W. Li, *Adv. Mater.*, 2016, **28**, 943-950.

3 J. W. Jung, J. W. Jo, C. C. Chueh, F. Liu, W. H. Jo, T. P. Russell and A. K. Jen, *Adv. Mater*., 2015, **27**, 3310.

4 L. Huo, T. Liu, B. Fan, Z. Zhao, X. Sun, D. Wei, M. Yu, Y. Liu and Y. Sun, *Adv. Mater*., 2015, **27**, 6969.

5 J. Subbiah, B. Purushothaman, M. Chen, T. Qin, M. Gao, D. Vak, F. H. Scholes, X. Chen, S. E. Watkins, G. J. Wilson, A. B. Holmes, W. W. H. Wong and D. J. Jones, *Adv. Mater*., 2015, **27**, 702.

6 (a) Z. Li, L. Ying, R. Xie, P. Zhu, N. Li, W. Zhong, F. Huang and Y. Cao, *Nano Energy*, 2018, **51**, 434; (b) C. R. McNeill, S. Westenhoff, C. Groves, R. H. Friend and N. C. Greenham, *J. Phys. Chem. C*, 2007, **111**, 19153.

7 A. K. Kyaw, D. H. Wang, D. Wynands, J. Zhang, T. Q. Nguyen, G. C. Bazan and A. J. Heeger, *Nano Lett.*, 2013, **13**, 3796.

8 L. Lu, W. Chen, T. Xu and L. Yu, *Nat. Commun.*, 2015, **6**, 7327.

9 S. R. Cowan , A. Roy and A. J. Heeger , *Phys. Rev. B*, 2010, **82**, 245207.

10 C. Waldauf, M. C. Scharber, P. Schilinsky, J. A. Hauch and C. J. Brabec, *J. Appl. Phys.*, 2006, **99**, 104503.

11 S. Yoo, B. Domercq and B. Kippelen, *J. Appl. Phys.*, 2005, **97**, 103706.

12 N. Li, D. Baran, G. D. Spyropoulos, H. Zhang, S. Berny, M. Turbiez, T. Ameri, F. C. Krebs and C. J. Brabec, *Adv. Energy Mater.*, 2014, **4**, 1400084.